Behavior of the interaction between twin transitional round fountains in a homogeneous fluid, Part 1: Experimental study

Hasan Mahmud[a], Wenxian Lin[1a,b], Wenfeng Gao[b], Blair Hill[a], S. W. Armfield[c], Yinghe He[a]

[a] *College of Science, Technology & Engineering, James Cook University, Townsville, QLD 4811, Australia*
[b] *Solar Energy Research Institute, Yunnan Normal University, Kunming, Yunnan 650092, P. R. China*
[c] *School of Aerospace, Mechanical and Mechatronic Engineering, The University of Sydney, NSW 2006, Australia*

Abstract

The interaction of multiple sourced fountains is very common in many applications such as computers and electronic instruments, discharge of waste water from power plants to marine environments, displacement ventilation and air conditioning of large building spaces. But the understanding of such an interaction is currently scarce. This paper is the first part of the study on the behavior of the interaction between twin transitional round fountains with equal power in a homogeneous fluid. In this paper, the interaction behavior is investigated experimentally using a noninvasive PIV technique and flow visualization over the ranges $25 \leq Re \leq 400$ and $1 \leq Fr \leq 5$ at the fixed spacing of $D/X_0 = 10$, where Re and Fr are the Reynolds and Froude numbers, D is the spacing between the two fountain sources, and X_0 is the radius of orifices at the fountain source. The interaction behavior is observed to be dominated by bobbing and flapping motions and is either steady, or unsteady and weakly multi-modal or strongly multi-modal, depending on the specific values of Re and Fr. In a steady interaction, the bobbing-flapping motions are only present in its initial development stage and the interaction will attain a steady state in the later development stage in which the bobbing-flapping motions are no longer present and the maximum

[1]Corresponding author: Email: wenxian.lin@jcu.edu.au, Phone: +61-7-4781-5091, Fax: +61-7-4781-6788 (W. Lin)

interaction height, z_i, becomes constant. In an unsteady interaction, the interaction remains unsteady all the time and the bobbing-flapping motions are present at all development stages. The unsteady interaction is characterised by a finite number of discrete modes, with the time averaged z_i approximately constant. Among all cases considered, the steady interaction behavior is observed for the cases of $Re \leq 100$ with all Fr values considered and of $Fr \leq 1$ with all Re values considered, except $Re = 400$; the unsteady weakly multi-modal interaction behavior is observed for $150 \leq Re \leq 300$ with $1.5 \leq Fr \leq 5$ and $Fr = 1$ with $Re = 400$; and the unsteady strongly multi-modal interaction behavior is found for $Re = 400$ with $1 < Fr \leq 5$. Dimensional analysis and the experimental results are also used to develop an empirical scaling relation between $\bar{z}_i$, which is the time-averaged dimensionless maximum interaction height at full development, and Re and Fr, *i.e.*, $\bar{z}_i = 0.194 Fr^{7/4} Re^{1/4}$ over the ranges $25 \leq Re \leq 400$ and $1 \leq Fr \leq 5$, at the fixed spacing of $D/X_0 = 10$.

Keywords: Transitional round fountain, Interaction behavior, Twin fountains, Bobbing, Flapping, PIV.

1. Introduction

Fountain flows are common in nature and in engineering applications due to their specific features, such as in natural ventilation, volcanic eruptions, cumulus clouds, and reverse cycle air-conditioning, to name just a few. When a dense fluid is injected upward into a less dense ambient fluid, or vice versa, when a light fluid is injected downward into a dense ambient fluid, a fountain flow forms.

The behavior of a free single fountain flow injected into a homogeneous fluid is governed by the Reynolds number, Re, and the Froude number, Fr, defined for a round fountain injected from an orifice source as follows,

$$Re = \frac{W_0 X_0}{\nu}, \quad Fr = \frac{W_0}{\sqrt{X_0 g \Delta\rho/\rho_0}}, \tag{1}$$

where X_0 is the radius of the orifice, W_0 is the average velocity of the fountain fluid at the source, g is the acceleration due to gravity, ν is the kinematic viscosity

of fluid, and $\Delta\rho$ is the density difference between that of the fountain fluid (ρ_0) and that of the ambient fluid (ρ_a).

Although the studies on fountains commenced in the 1950s (see, *e.g.*, [1]), they are still being extensively investigated (see, *e.g.*, [2–12]). However, the studies have focused on single fountains ejected from a single source. A single round fountain may be a 'very weak' one when its Fr is smaller than 1, or a 'weak' one when its Fr is in the range of $1 \leq Fr \leq 3$, or a 'forced' one when $Fr \geq 3$, as classified by [8, 13]. The behavior of a forced fountain is found to be significantly different from that of a weak or very weak fountain (see, *e.g.*, [3, 5, 8, 9, 13–19]), as summarized in [17].

The most common parameter used in characterizing fountain flow behavior is Z_m, which is the maximum fountain penetration height and is normally made dimensionless by the source radius X_0, *i.e.*, $z_m = Z_m/X_0$. For forced round fountains ejected from an orifice into a homogeneous fluid, the time-averaged z_m, *i.e.*, $\bar{z}_m$, is usually used, and it has been found that

$$\bar{z}_m = CFr, \tag{2}$$

where C is a constant of proportionality. Although a variety of C values have been obtained under considerably different conditions (see, *e.g.*, [1, 19–22]), $C = 2.46$, which was determined by Turner [23] using dimensional analysis and experiments, has been found to be the most likely value, as confirmed by a series of subsequent studies (see *e.g.*, [13, 24, 25]). The readers are referred to, *e.g.*, [2, 6–8, 11, 17, 18, 23, 26–30], for some earlier and recent studies on the characteristics of forced round fountains.

Kaye & Hunt [13] and Burridge & Hunt [8] proposed the following scalings for $\bar{z}_m$ based on their extensive experimental results:

$$\bar{z}_m = \begin{cases} 0.81Fr^{2/3} & \text{for } 0.4 \leq Fr \leq 1 \text{ and } 924 \leq Re \leq 2171, \\ 0.86Fr^2 & \text{for } 1 \leq Fr \leq 2.8 \text{ and } 1015 \leq Re \leq 2780, \\ 2.46Fr & \text{for } Fr > 2.8 \text{ and } 969 \leq Re \leq 4022. \end{cases} \tag{3}$$

Some of these scalings were also obtained by several other studies (see, *e.g.*, [15, 31]).

For laminar and transitional round fountains the consensus seems to be that in addition to the momentum flux and buoyancy flux the fluid viscosity also plays an important role [13, 16, 18, 31, 32], leading to the assumption that $\bar{z}_m$ is also under the influence of Re, *i.e.*,

$$\bar{z}_m = C_1 Fr Re^n, \tag{4}$$

where n is a constant, which is found to be dependent on Fr and Re, and C_1 is a constant of proportionality. However, different n values have been obtained for round fountains with different values of Fr and Re. For example, for $Fr \sim 1$ and $Re \leq 500$, Lin & Armfield [16] obtained $n = -1/2$ with scaling analysis and direct numerical simulation results, whereas Philippe *et al.*[32] and Williamson *et al.*[18] obtained $n = 1/2$ based on experimental results. For very weak fountains with $Fr \ll 1$, Lin & Armfield [15] speculated that the inertia effect is very small and the fountain flow behavior is predominantly controlled by the buoyancy flux and the fluid viscosity and obtained $n = -2/3$ using dimensional consistency, which was confirmed by their direct numerical simulation results as well as by the analytical and experimental results of Kaye & Hunt [13], as noted above.

The interaction of multiple sourced jets/plumes is an important phenomenon in many applications such as cooling and heating in food industry, computers and electronic instruments, flow rising from industrial and households smokestacks, displacement ventilation and air conditioning of large building spaces, etc. There have been many investigations on this topic (see, *e.g.*, [33–38]). One particular type of interaction of multiple sourced jets/plumes is the 'filling-box' and 'emptying filling-box' problems which have attracted a considerable interest since the analytical study of Baines & Turner [39] on this topic. The understanding of such flows is of significance in improving the efficient design of naturally ventilated spaces [40], mixing in oceanographic applications [41], among many others, and many studies have been carried out on it. For example, Cooper & Linden[42] analysed the interaction of two plumes with both buoyancy of the same sign and of the opposite sign within a naturally ventilated enclosure containing two point sources of buoyancy and developed a model to predict the thermal stratification

caused by the interaction of the two plumes produced, which was confirmed by their experimental results; Linden & Cooper [43] further developed an approximate model for the flow and stratification within a naturally ventilated enclosure containing multiple sources of buoyancy; Kaye & Linden [44, 45] investigated the coalescence of two co-flowing axisymmetric turbulent plumes and the collision of two axisymmetric turbulent plumes with buoyancy fluxes of opposite sign and developed models for the interactions of two plumes under various configurations and conditions based on the ventilation model of Linden, Lane-Serff & Smeed [46] which are shown to be in good agreement with their experimental results; Wong & Griffiths [47] extended these studies by developing a generalized filling-box model to account for the multiple non-interacting sources of unequal strength, whereas very recently, Shrinivas & Hunt [48] examined theoretically the transient displacement flow and density stratification that develops within a ventilated box after two localized floor-level heat sources of unequal strengths are activated. The readers are referred to [41, 47, 48] for a review of some of these studies on the topic.

Nevertheless, all these studies have been on the interactions of two or multiple plumes or jets. To our best knowledge, no study has been found that investigates the interaction among multiple fountains, although they also have numerous applications. This motivates us to conduct the current study on the behavior of the interaction of twin transitional round fountains in a homogeneous fluid. The fountains under consideration have identical powers and are ejected at the same direction from two identical round orifices with a finite spacing, as schematically shown in Fig. 1. The present paper is the first part of this study which reports the experimental investigation of the interaction behavior of twin fountains over the ranges $25 \leq Re \leq 400$ and $1 \leq Fr \leq 5$ with the distance between the two fountain sources fixed at $D/X_0 = 10$, where D is the spacing between the two fountain sources. The experiments were carried out using flow visualization and non-invasive PIV techniques. The experimental results demonstrate that bobbing and flapping motions, which are respectively the vertical and horizontal motions of the peak point of the interface between the interaction region and the ambient

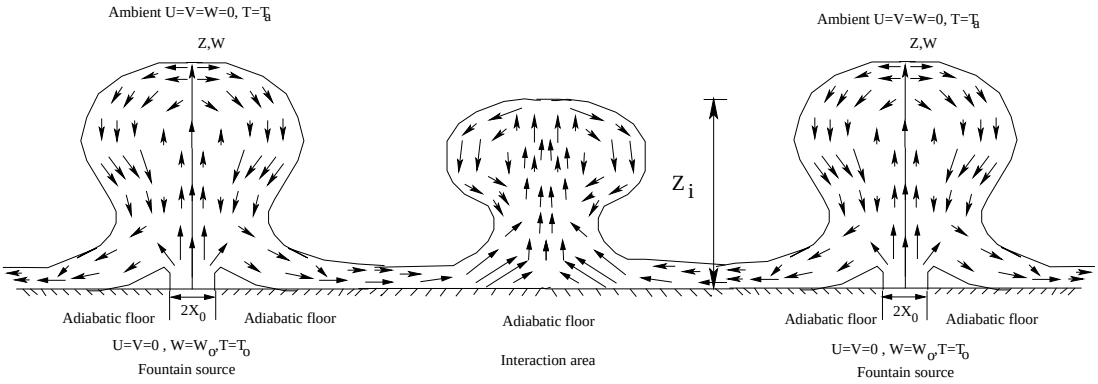

Figure 1: Schematic of the interaction of twin fountains.

fluid on the vertical plane passing through the twin fountain sources, are the dominant characteristics of the interaction behavior. However, due to the restrictions imposed by the experimental setup and conditions, the ranges of Re and Fr as well as the distance between the two fountain sources which the experiments were able to cover, are significantly limited. To explore the interaction behavior of twin fountains over much wider ranges of Re and Fr and at different distances between the two fountain sources, a numerical study was also carried out over the ranges of $1 \leq Fr \leq 10$ and $25 \leq Re \leq 1000$ and at varied distances between the two fountain sources with a series of three-dimensional direct numerical simulation, which, as the second part of the current study, is accompanied but will be reported separately in this journal [49].

The remainder of this paper is organized as follows. The experimental setup and details are described in § 2. The experimental observation of the behavior of the interaction between the twin transitional round fountains and the experimental results on the maximum fountain penetration heights and thickness of the interaction region are presented and discussed in § 3. Finally, the conclusions are made in § 4.

2. Experimental details

Under consideration is the behavior of the interaction of twin transitional round fountains with equal power in a homogeneous fluid. A series of exper-

iments were conducted over the ranges of $25 \leq Re \leq 400$ and $1 \leq Fr \leq 5$ at $D/X_0 = 10$ using a high-framing-rate stereo PIV (HFR-SPIV) system, from Dantec Dynamics, with only a single camera. In these experiments, twin round fountains were produced by injecting, through two identical round orifices which is separated by a spacing of D, saline water vertically upwards into fresh water contained in a 1m $\times$ 1m $\times$ 0.6m Perspex-sided test tank as depicted in Fig. 2, where the experimental setup is shown.

Prior to the commencement of each experiment, the salt water tank was filled with fresh water. High quality salt and almost neutrally buoyant Nylon 12 Polyamide polymer spherical tracer particles (density 1030 kg/m^3, mean diameter 50 μm) were added into the salt water tank and well mixed using a Davey D15A submersible sump pump to achieve the desired uniform density of the saline water for a specific Froude number of the experiment. The Perspex-sided test tank was filled with fresh water from the mains up to the desired height, and Nylon 12 Polyamide polymer spherical tracer particles were also added and well mixed. After the saline water and the fresh water in both tanks became stationary, their individual densities were measured by a hand-held Mettler Toledo Densito 30PX density meter which had an accuracy of $\pm$ 1 kg/m^3, a resolution of 0.1 kg/m^3, and the measurement range of 0 $\sim$ 2000 kg/m^3.

A twin fountain flow was initiated by opening the ball valve to eject saline water into the test tank at a fixed flow rate for the specific Reynolds number using the sump pump, and this flow was maintained in the course of the experiment. The volumetric flow rate was measured and controlled by an Aalborg high precision needle valve flow meter. In order to avoid clogging of seeded particles inside the flow meter, a water filter was installed before the entry section of the meter. The saline water inlet pipes were aligned flush with the floor of the fresh water tank and were kept long enough to ensure that the flow entering the test tank was fully developed. A small amount of food dye was used for visualizing fountain flows. The flow visualization images were obtained by a Sony Digital HD Video Camera Recorder (Model: HDR-PJ760VE, 24.1 Megapixels). These images were recorded simultaneously with the PIV image-capturing, with the flow

Table 1: Key data for the PIV experiment runs.

Run	Fr	Re	Q (mL/min)	W_0 (m/s)	ρ_0 (kg/m^3)	ρ_a (kg/m^3)
1	1	25	45.103	0.0024	998.9	998.8
2	1	50	90.205	0.0048	998.7	998.5
3	1	75	135.308	0.0073	998.9	998.4
4	1	100	180.410	0.0096	999.4	998.5
5	1	200	360.821	0.0191	1002.1	998.4
6	1	300	541.231	0.0287	1006.5	998.1
7	1	400	721.641	0.0383	1013.0	998.1
8	2	50	90.2052	0.0048	998.3	998.2
9	2	75	135.308	0.0072	998.8	998.7
10	2	100	180.410	0.0096	999.1	998.9
11	2	200	360.821	0.0191	999.5	998.6
12	2	300	541.231	0.0287	1000.7	998.6
13	2	400	721.641	0.0383	1002.1	998.4
14	3	100	180.410	0.0096	998.3	998.2
15	3	200	360.821	0.0191	998.6	998.3
16	3	300	541.231	0.0287	999.4	998.6
17	3	400	721.641	0.0383	1000.2	998.5
18	4	100	180.410	0.0096	998.0	997.9
19	4	200	360.821	0.0191	998.1	997.9
20	4	300	541.231	0.0287	998.3	997.9
21	4	400	721.641	0.0383	998.8	998.0
22	5	100	180.410	0.0096	998.7	998.6
23	5	200	360.821	0.0191	998.8	998.6
24	5	300	541.231	0.0287	999.1	998.8
25	5	400	721.641	0.0383	999.1	998.5
26	1.5	150	270.616	0.0144	999.3	998.4
27	2.5	300	541.231	0.0287	999.5	998.2
28	3.5	400	721.641	0.0383	999.4	998.2
29	4.5	300	541.231	0.0287	998.9	998.5

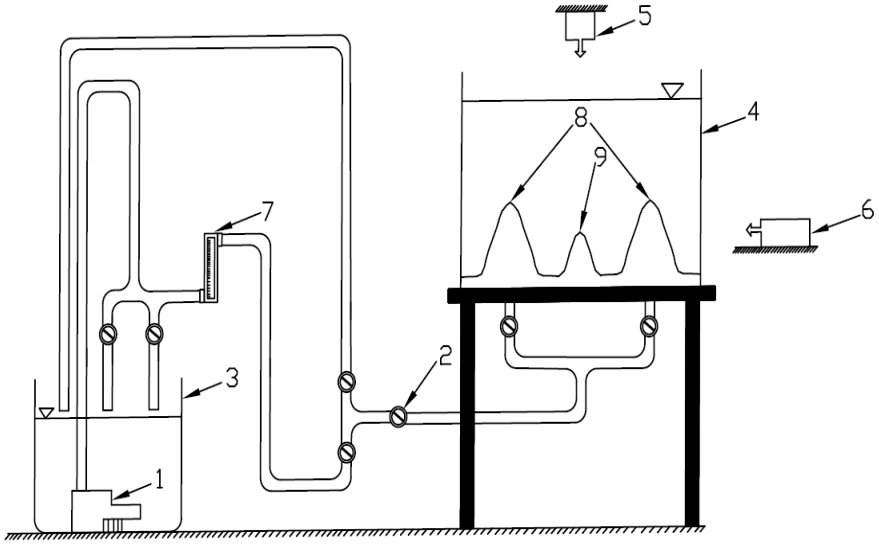

Figure 2: Schematic of the experimental setup: 1 - saline water supply pump; 2 - ball valve; 3 - saline water tank; 4 - fresh water test tank; 5 - double pulsed Nd: Yag laser source; 6 - high resolution CCD camera; 7 - needle valve flow meter; 8 - twin fountains formed; 9 - interaction region of twin fountains.

field of interest being illuminated by the laser sheet.

Experimental ranges of Fr and Re were varied by adjusting the salinity of the saline water and the inlet flow rate of the fountains at the sources, which were orifices with constant radius $X_0 = 10$ mm, with the volumetric rates varying from 45.103 ml/min to 721.641 ml/min and the density ratio $(\rho_0 - \rho_a)/\rho_a$ (ρ_0 for saline water and ρ_a for fresh water, both at the fountain sources) varying from 2×10^{-5} to 1.47×10^{-2}. Totally 29 experimental runs were carried out, with the key data for each of these runs listed in Table 1. Both fountain sources were located 50 mm away from the bottom centre of the test tank.

It should be noted that the ranges of Re and Fr and other variables were limited by the restrictions imposed by the experimental setup and conditions in this work. As X_0 was fixed at 10 mm and D at 100 mm due to the experimental setup, the maximum Fr was limited to be no more than 5 due to the accuracy of $\pm$ 1 kg/m^3 and the resolution of 0.1 kg/m^3 the hand-held Densito 30PX Density Meter. For example, at $Re = 500$, the required flowrate for $Fr = 6$ would be

about 950 mL/min and the density difference ($\rho_0 - \rho_a$) between the saline water and the fresh water would be 0.007 kg/m^3 only, which is much smaller than the resolution of the density meter. The maximum Re is limited to be no more than 400 due to the use of the Aalborg high precision needle valve flow meter in the experimental setup, which only has the practical range to measure reliably a maximum flowrate of about 900 mL/min. Hence, the maximum Fr and Re achieved with the current experimental setup and conditions in this work are 5 and 400, respectively. As the fountains with $Fr < 1$ and $Re < 25$ are beyond the scope of this work, the experiments were therefore conducted over the ranges of $25 \leq Re \leq 400$ and $1 \leq Fr \leq 5$. As only one test tank with $D = 100$ mm and $X_0 = 10$ mm was manufactured for the experimental setup, the experiments were also limited to only one single spacing of $D/X_0 = 10$.

The FlowManager of the Dantec PIV device controls the duration of the PIV experiment, the image capturing of the high speed camera (a Redlake HG-100K camera with a maximum resolution of 1504×1128 pixels and at a high framing rate of 1,000 fps), and the operation of the double pulsed laser (a Lee LDP-100MQG Nd: YAG laser emitting 0.532 μm radiation). The reader is referred to [50] for the detailed description of the PIV device and the Flow-Manager software, which has the image-capturing software built in it.

3. Experimental results

3.1. Observed behavior of interaction

For all cases studied in this work, the behavior of the interaction of twin transitional round fountains is observed to be characterized by bobbing and flapping motions, as will be detailed below. Based on the characteristics of these bobbing and flapping motions, the interaction behavior of the twin transitional round fountains, over the ranges of Re and Fr considered and at the fixed spacing of $D/X_0 = 10$, may be characterised in three regimes; (a) a steady regime in which the bobbing and flapping motions are only present at the early development stage and disappear at the later fully developed stage. This behavior

is mainly observed in the lower Re/Fr cases studied. For brevity, such an interaction behavior is hereinafter denoted as a 'steady interaction' in this study; (b) an unsteady weakly multi-modal regime in which the bobbing and flapping motions are present at every stage of the flow development and at full development, are comprised of three or fewer modes. This behavior is mainly observed in the intermediate Re/Fr cases studied, and is hereinafter denoted as a 'weakly multi-modal interaction'; and (c) an unsteady strongly multi-modal regime in which the bobbing and flapping motions are also present at every stage of the flow development, and are comprised of a large number of discrete modes. Such a behavior is mainly observed in the higher Re/Fr cases studied.

3.1.1. Steady interaction behavior

Among all cases considered in the experiments, there are several cases with lower Re/Fr values in which the bobbing and flapping motions are only present at the early, start-up stage of the development and disappear at the later stage, and the flow is steady at full development. Such a steady interaction is observed for the cases of $Re \leq 100$ with all Fr values considered and of $Fr = 1$ with all Re values, except $Re = 400$, considered, as shown in Fig. 3 where the $Fr - Re$ regime map for the interaction behavior observed in this paper is illustrated. It is apparent that demarcation curves can be found to distinguish the three regime of the interaction behavior, although the exact locations of such curves cannot be determined here due to the limitations experienced with the experiments.

The steady interaction behavior is shown, as an example, by the flow visualization images at different times, in Fig. 4 for the case of $Fr = 1$ and $Re = 100$. A much clearer illustration of the behavior is shown in the corresponding time series of u_i, w_i, and z_i of the interaction, and the corresponding power spectra of u_i and w_i, which were obtained by the discrete Fourier transform, in Fig. 5, where u_i and w_i are the dimensionless horizontal and vertical velocities at the peak point of the interface between the interaction region and the ambient fluid on the vertical plane passing through the twin fountain sources, and z_i is the dimensionless height of this same peak point. u_i, w_i, and z_i are made dimensionless by the

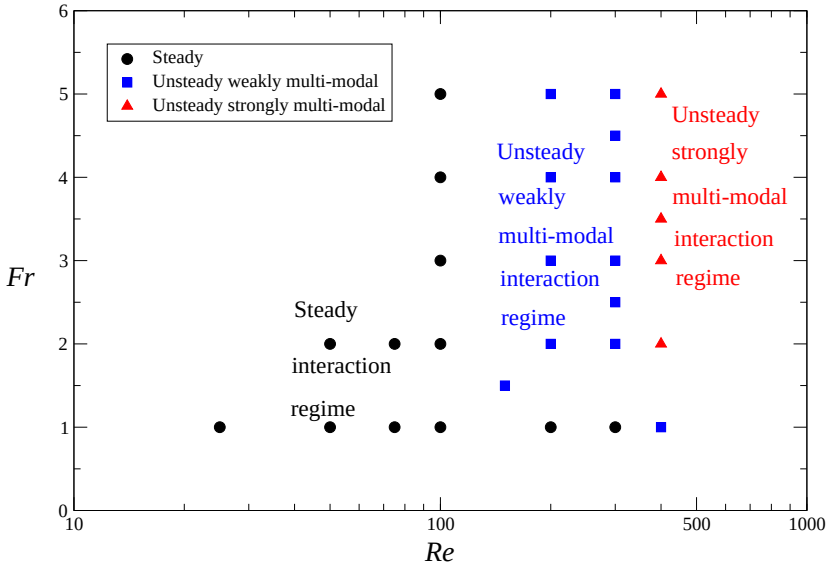

Figure 3: $Fr - Re$ regime map for the interaction behavior of twin transitional round fountains at the fixed spacing of $D/X_0 = 10$.

characteristic velocity W_0 and the characteristic length X_0, respectively. The development of the interaction region is initially oscillatory in both the horizontal direction (due to the flapping behavior) and the vertical direction (due to the bobbing behavior), with gradually reduced magnitudes of oscillations, as shown in Figs 5(a) and 5(c), respectively, until at $\tau \approx 180$ when the interaction reaches its fully developed, steady state the bobbing and flapping motions disappear, and all quantities are constant.

When Fr is increased but Re is kept low, the interaction is still steady at the fully developed stage, but a slightly varied interaction behavior is observed. The flapping and bobbing motions with gradually reduced magnitudes of oscillations are also present in the initial development of the interaction and disappear when the interaction attains its steady state. However, the increase in Fr leads to an increased mixing of the fountain fluid with the ambient fluid, a higher interaction region, much stronger unsteadiness in the fountain intrusions and the associated interaction, as demonstrated, as an example, by the flow visualization images in Fig. 6 and the corresponding time series of u_i, w_i, and z_i of the interaction in Fig. 7 for the case of $Fr = 4$ and $Re = 100$. Another difference, although not very

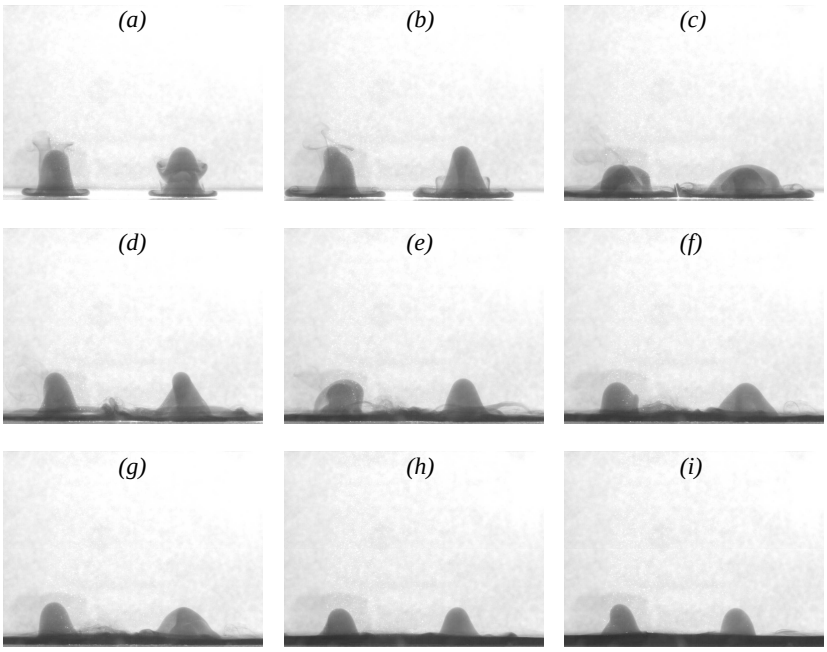

Figure 4: Typical flow visualization images showing the time evolution of a steady interaction behavior of the twin round fountains with $Fr = 1$ and $Re = 100$ at (a) $\tau = 8.93$, (b) $\tau = 12.12$, (c) $\tau = 16.59$, (d) $\tau = 19.79$, (e) $\tau = 25.53$, (f) $\tau = 32.55$, (g) $\tau = 43.83$, (h) $\tau = 88.09$, and (i) $\tau = 166.82$, respectively, where time τ is made dimensionless by X_0/W_0, which is the characteristic time scale for the fountains.

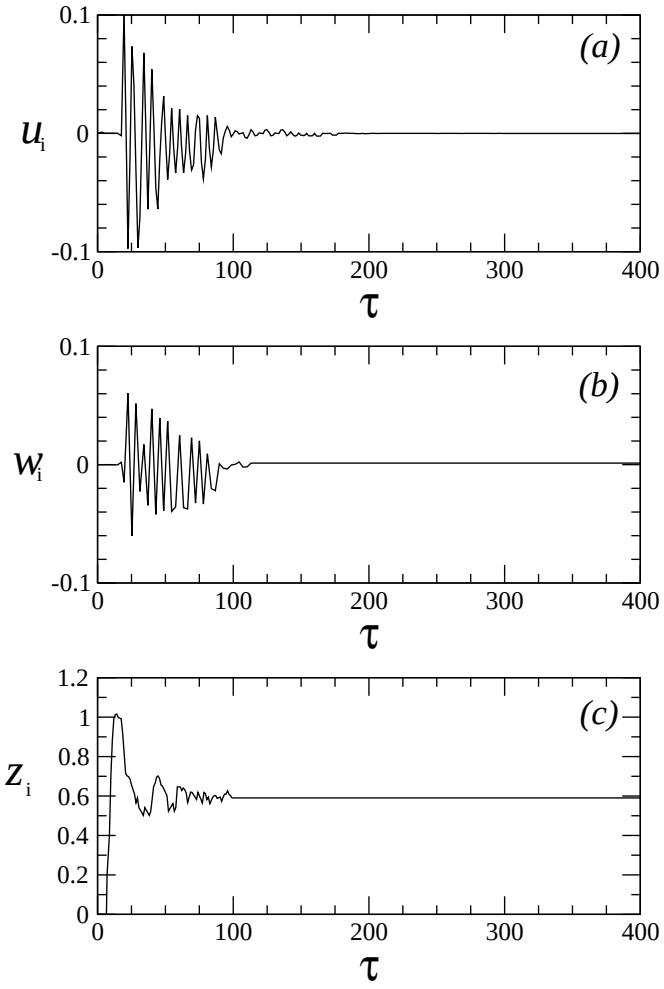

Figure 5: Time series of (a) u_i, (b) w_i, and (c) z_i of the twin round fountains at $Fr = 1$ and $Re = 100$ which demonstrate a steady interaction behavior.

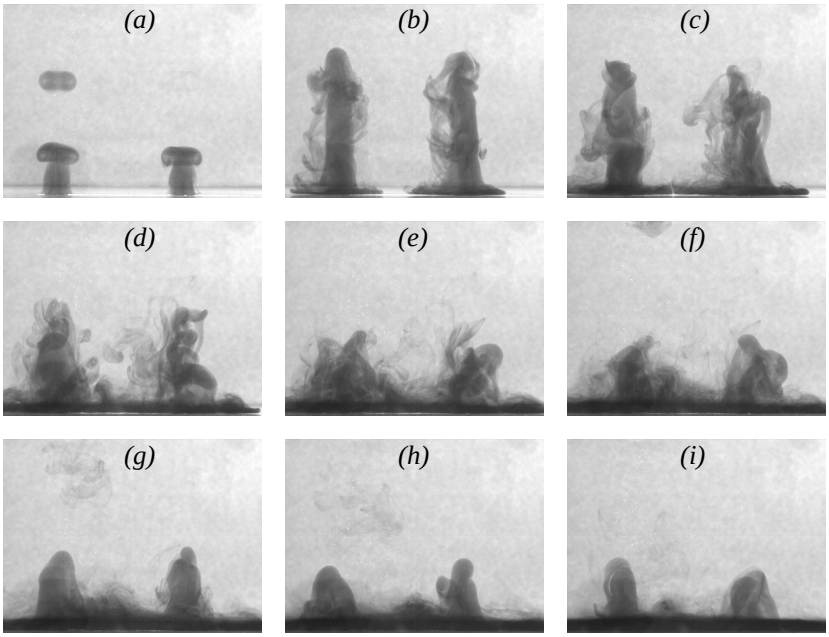

Figure 6: Typical flow visualization images showing the time evolution of a steady interaction behavior with $Fr = 4$ and $Re = 100$ at (a) $\tau = 38.72$; (b) $\tau = 48.19$; (c) $\tau = 57.53$; (d) $\tau = 71.49$; (e) $\tau = 86.60$; (f) $\tau = 106.17$; (g) $\tau = 134.05$; (h) $\tau = 148.24$; and (i) $\tau = 171.05$, respectively.

significant and the relevant experimental results are not presented in the figure, is that in the steady interaction with a larger Fr, a three-dimensional feature is also present, *i.e.*, v_i, which is the velocity in the third direction at the peak point, is not zero in the initial development of the interaction, although its magnitude is not significant and it becomes zero when the interaction attains the steady state. In the steady interaction with a small Fr, however, v_i is negligible at any instant of the development of the interaction.

3.1.2. Unsteady weakly multi-modal interaction behavior

The unsteady weakly multi-modal interaction behavior is observed for the cases of $1.5 \leq Fr \leq 5$ with $150 \leq Re \leq 300$ and $Fr = 1$ with $Re = 400$, among all cases considered in the experiments.

The unsteady weakly multi-modal interaction behavior is demonstrated, as an example, by the flow visualization images at different times in Fig. 8 and the corresponding time series of u_i, w_i, and z_i of the interaction as well as the

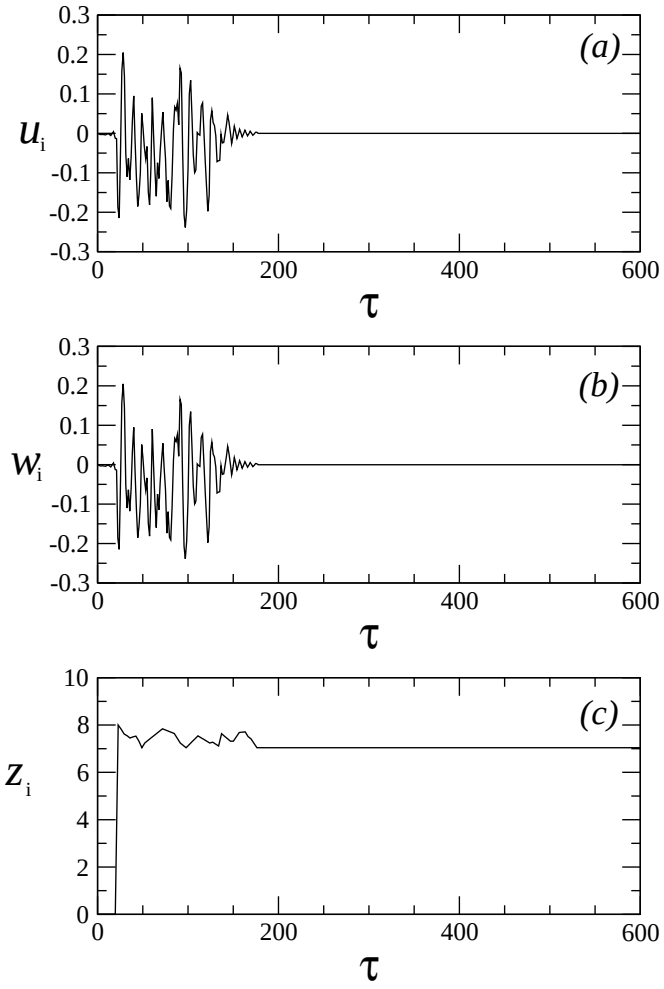

Figure 7: Time series of (a) u_i, (b) w_i, and (c) z_i of the twin round fountains at $Fr = 4$ and $Re = 100$ which demonstrate a steady interaction behavior.

corresponding power spectra of u_i and w_i, which were obtained by the discrete Fourier transform, in Fig. 9 for the case of $Re = 300$ and $Fr = 3$. In this regime, the bobbing and flapping motions are present at every stage of the start-up and full development of the interaction, as clearly shown in Figs. 9(a) and 9(c). The magnitudes of the oscillations of both the bobbing and flapping motions become almost constant in the later stages of the time series, showing that the flow is then fully developed. Initially the oscillations increase to a magnitude greater than their fully developed values, with subsequent decay, particularly noticeable for z_i. z_i oscillates around an almost constant time-averaged value (about 5.6) at the fully developed stage, as shown in Fig. 9(e). The flapping motions are dominated by two dimensionless frequencies, $f \approx 0.09$ and $f \approx 0.044$, as shown in Fig. 9(b). The frequencies are dimensionless as they are obtained by FFT from the time series of u_i in which the time τ is made dimensionless by X_0/W_0, implying that the frequencies for u_i, as well as for w_i, are made dimensionless by W_0/X_0. The bobbing motions are dominated by only a single dimensionless frequency, at $f \approx 0.09$, as shown in Fig. 9(d). However, the time-averages of the oscillations of both the bobbing and flapping motions become negligible at the later stage of the development (over the time period from 300 to 600, the time-averaged u_i and w_i are found to be 0.01 and -0.03, respectively, which are much smaller than their respective maximum oscillation magnitudes, as shown in Figs. 9(a) and 9(c)).

As stated above, the unsteady weakly multi-modal interaction behavior is observed for $1.5 \leq Fr \leq 5$ with $150 \leq Re \leq 300$ and $Fr = 1$ with $Re = 400$, among all cases considered here. Another example to illustrate such behavior is presented in Fig. 10 for the case of $Fr = 2$ and $Re = 200$. Again the bobbing and flapping motions are present at all stages of the development of the interaction, as clearly shown in Figs. 10(a) and 10(c), and the magnitudes of the oscillations of both the bobbing and flapping motions also become almost constant in the later stages. Again the time-averages of the oscillations of both the bobbing and flapping motions become negligible at the fully developed stage (over the time period from 300 to 500, the time-averaged u_i and w_i are found to be 0.001 and

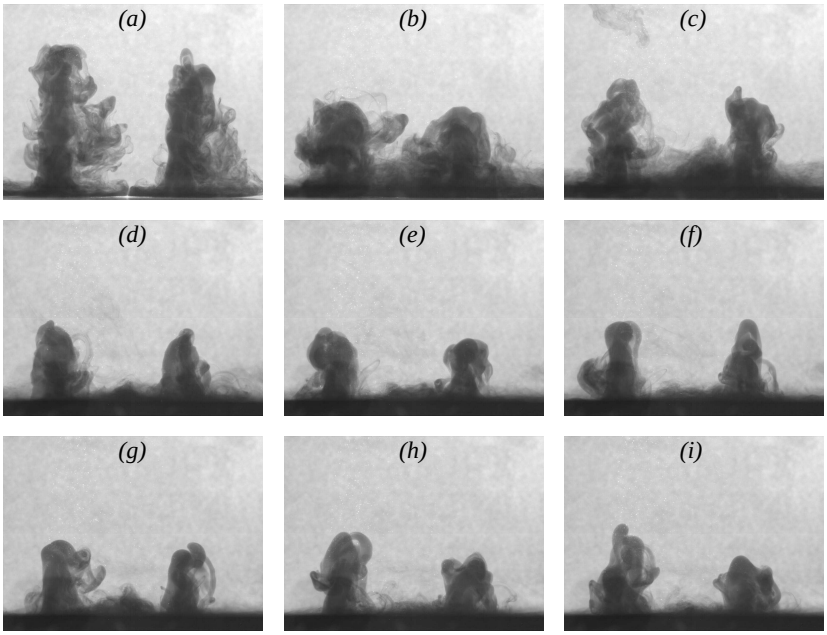

Figure 8: Typical flow visualization images showing the time evolution of an unsteady weakly multi-modal interaction behavior with $Fr = 3$ and $Re = 300$ at (a) $\tau = 29.36$, (b) $\tau = 45.96$, (c) $\tau = 62.56$, (d) $\tau = 160.18$, (e) $\tau = 190.06$, (f) $\tau = 229.16$, (g) $\tau = 249.85$, (h) $\tau = 291.08$, and (i) $\tau = 324.28$, respectively.

-0.028, respectively, which are also much smaller than the respective maximum magnitudes of the oscillations, as shown in Figs. 10(a) and 10(c)). z_i again oscillates around an almost constant time-averaged value (about 2.5 in this case) at the fully developed stage, as shown in Fig. 10(e). The flapping motions in this case are dominated by three dimensionless frequencies, at $f \approx 0.103$, $f \approx 0.053$ and $f \approx 0.126$, as shown in Fig. 10(b), with the first two dominant frequencies higher than those in the case of $Fr = 3$ and $Re = 300$. The bobbing motions are again dominated by a single frequency at $f \approx 0.13$, as shown in Fig. 10(d), which is also higher than that in the case of $Fr = 3$ and $Re = 300$. It is also evident that a similar unsteady weakly multi-modal interaction behavior is present in the $Re = 400$ and $Fr = 1$ case, as shown by the typical flow visualization images presented in Fig. 11 and the corresponding time series of u_i, w_i, and z_i of the interaction and the power spectra of u_i and w_i presented in Figs. 12, with the description details omitted here to avoid repetition.

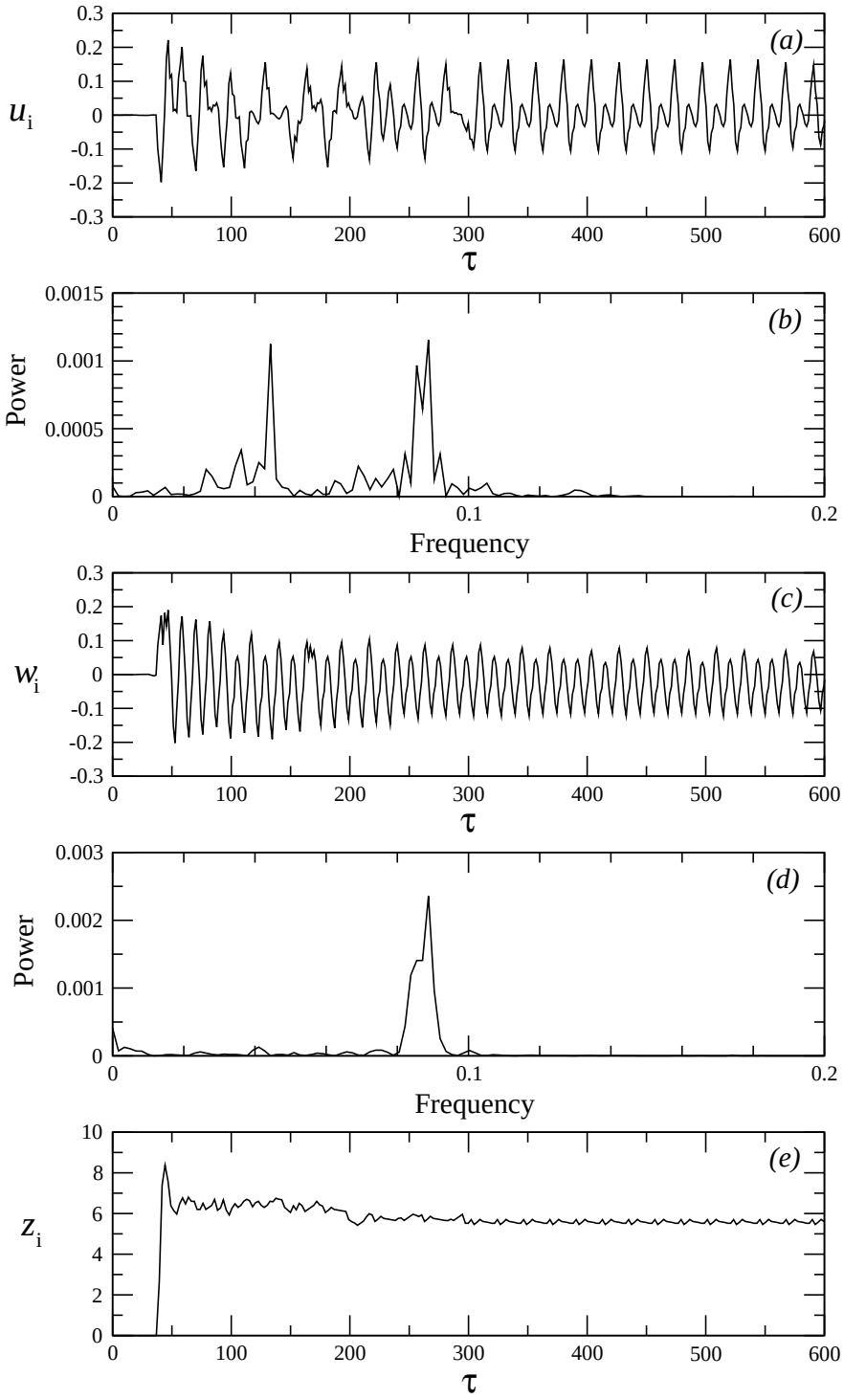

Figure 9: Time series of (a) u_i, (c) w_i, and (e) z_i of the twin round fountains at $Fr = 3$ and $Re = 300$ which demonstrate an unsteady weakly multi-modal interaction behavior, and the corresponding power spectra of u_i (b) and w_i (d), respectively.

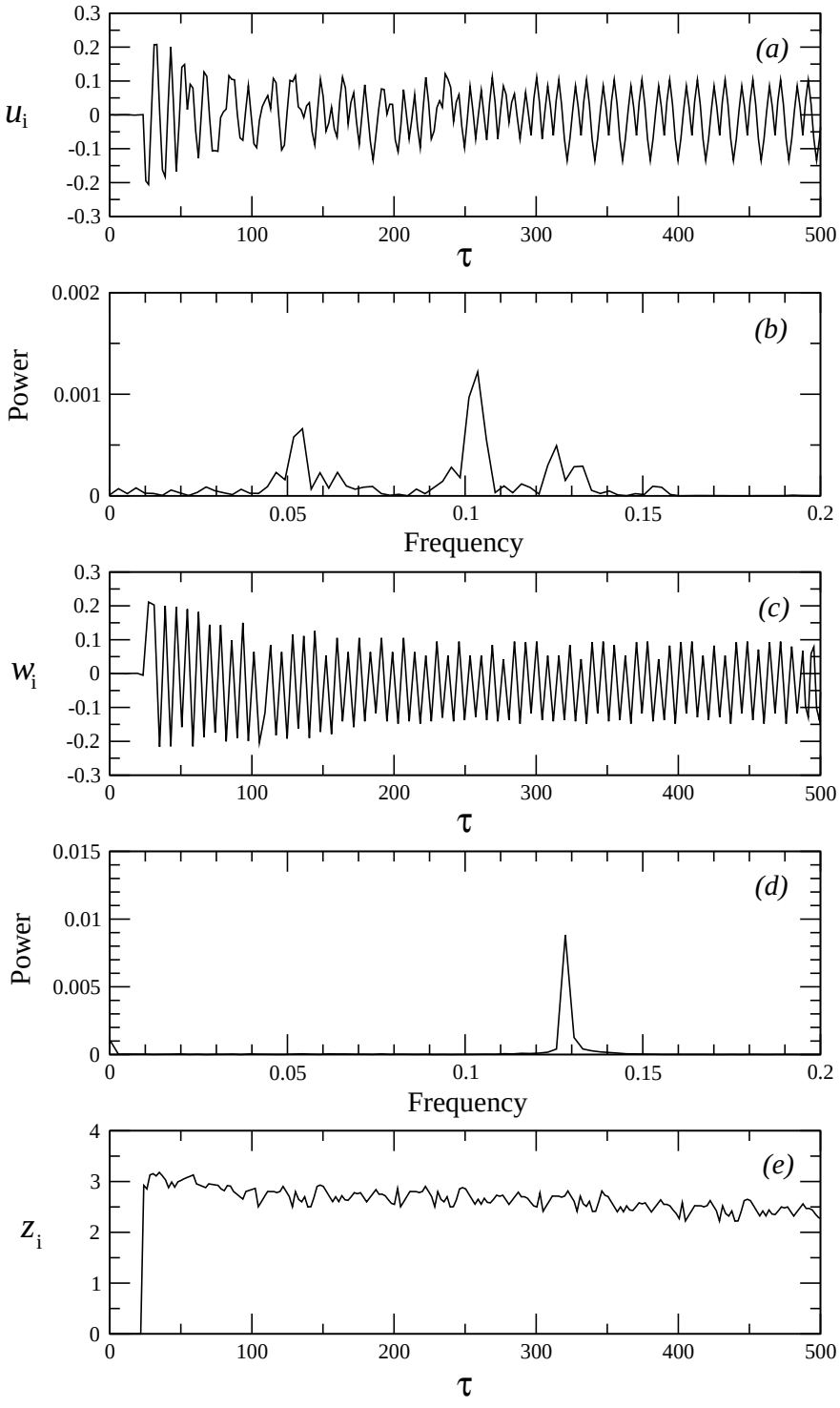

Figure 10: Time series of (a) u_i, (c) w_i, and (e) z_i of the twin round fountains at $Fr = 2$ and $Re = 200$ which demonstrate an unsteady weakly multi-modal interaction behavior, and the corresponding power spectra of u_i (b) and w_i (d), respectively.

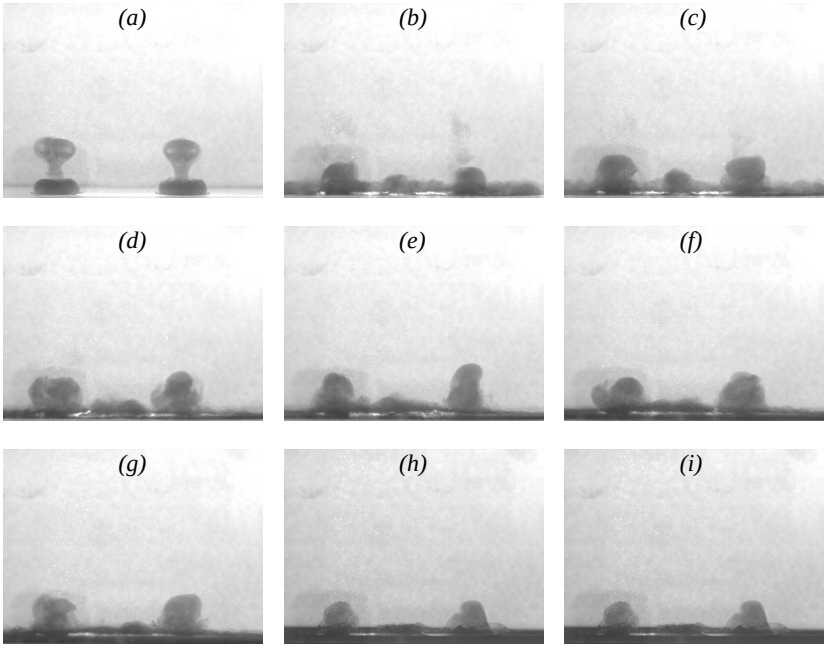

Figure 11: Typical flow visualization images showing the time evolution of an unsteady weakly multi-modal interaction behavior with $Fr = 1$ and $Re = 400$ at (a) $\tau = 5.10$; (b) $\tau = 12.76$; (c) $\tau = 15.32$; (d) $\tau = 20.42$; (e) $\tau = 26.81$; (f) $\tau = 35.74$; (g) $\tau = 48.51$; (h) $\tau = 191.92$; and (i) $\tau = 352.80$, respectively.

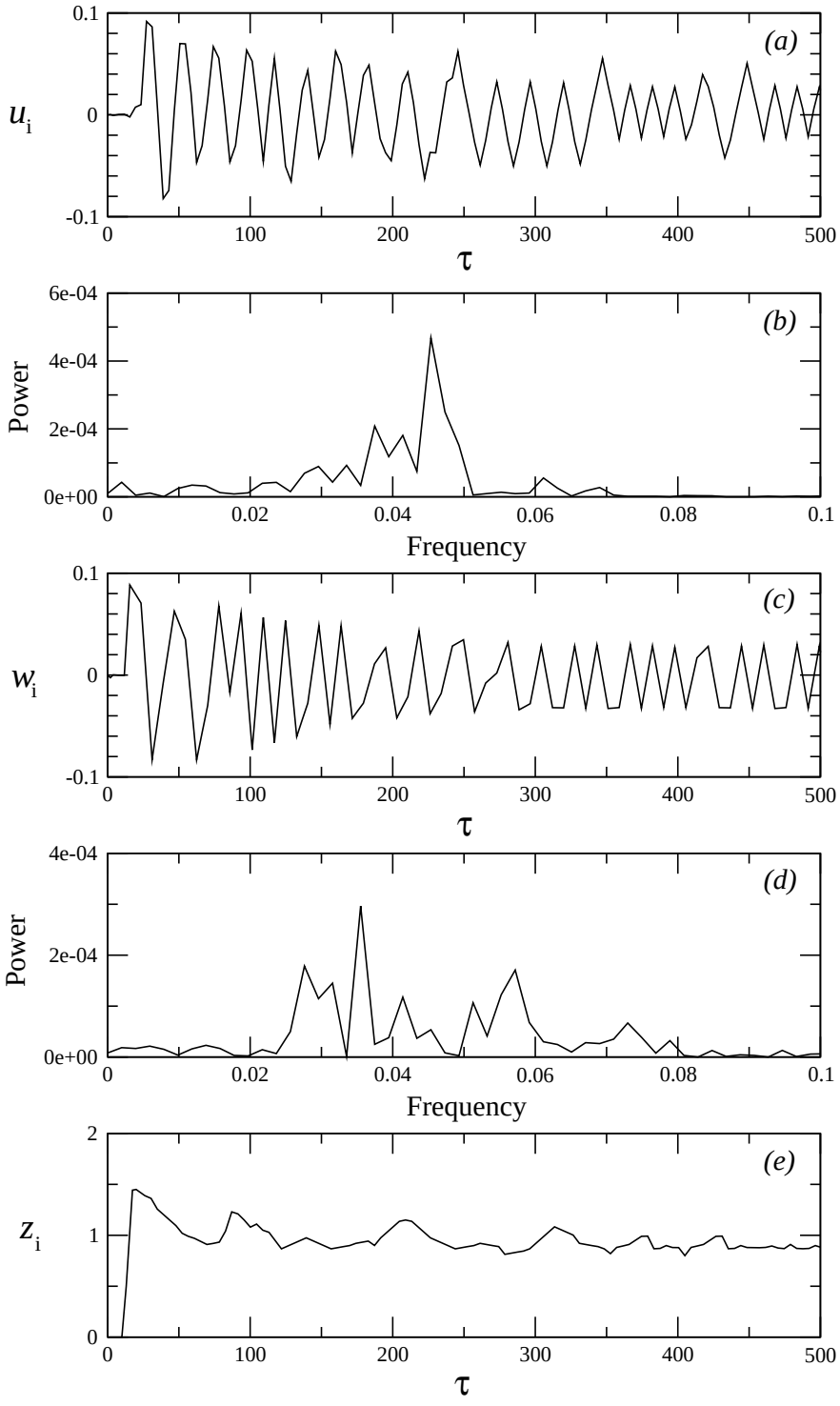

Figure 12: Time series of (a) u_i, (c) w_i, and (e) z_i of the twin round fountains at $Fr = 1$ and $Re = 400$ which demonstrate an unsteady weakly multi-modal interaction behavior, and the corresponding power spectra of u_i (b) and w_i (d), respectively.

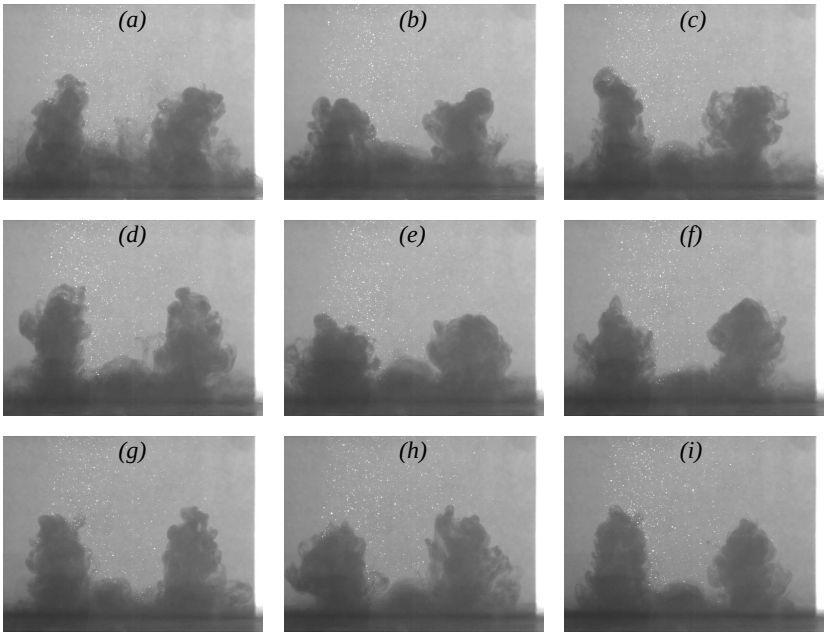

Figure 13: Typical flow visualization images showing the time evolution of an unsteady strongly multi-modal interaction behavior with $Fr = 3$ and $Re = 400$ at (a) $\tau = 78.94$; (b) $\tau = 99.16$; (c) $\tau = 109.37$; (d) $\tau = 132.14$; (e) $\tau = 166.65$; (f) $\tau = 190.66$; (g) $\tau = 240.17$; (h) $\tau = 280.71$; and (i) $\tau = 380.76$, respectively.

3.1.3. Unsteady strongly multi-modal interaction behavior

The unsteady strongly multi-modal interaction behavior is observed for $Re = 400$ with $1 < Fr \leq 5$, among all cases considered in this paper. This behavior can be illustrated, as an example, by the flow visualization images presented in Fig. 13 and the corresponding time series of u_i, w_i, and z_i of the interaction and the power spectra of u_i and w_i as shown in Fig. 14 for the case of $Re = 400$ and $Fr = 3$. From Fig. 14(b), it is observed that the flapping behavior is comprised of six significant frequencies, at $f \approx 0.039$, 0.06, 0.077, 0.098, 0.118, and 0.137, respectively. The spectra of the bobbing motions, shown in Fig. 14(d), is also comprised of at least six significant discrete frequencies. It is expected that with the further increase of Re and/or Fr, the number of discrete modes would increase further until, ultimately, the flapping and bobbing motions will become chaotic.

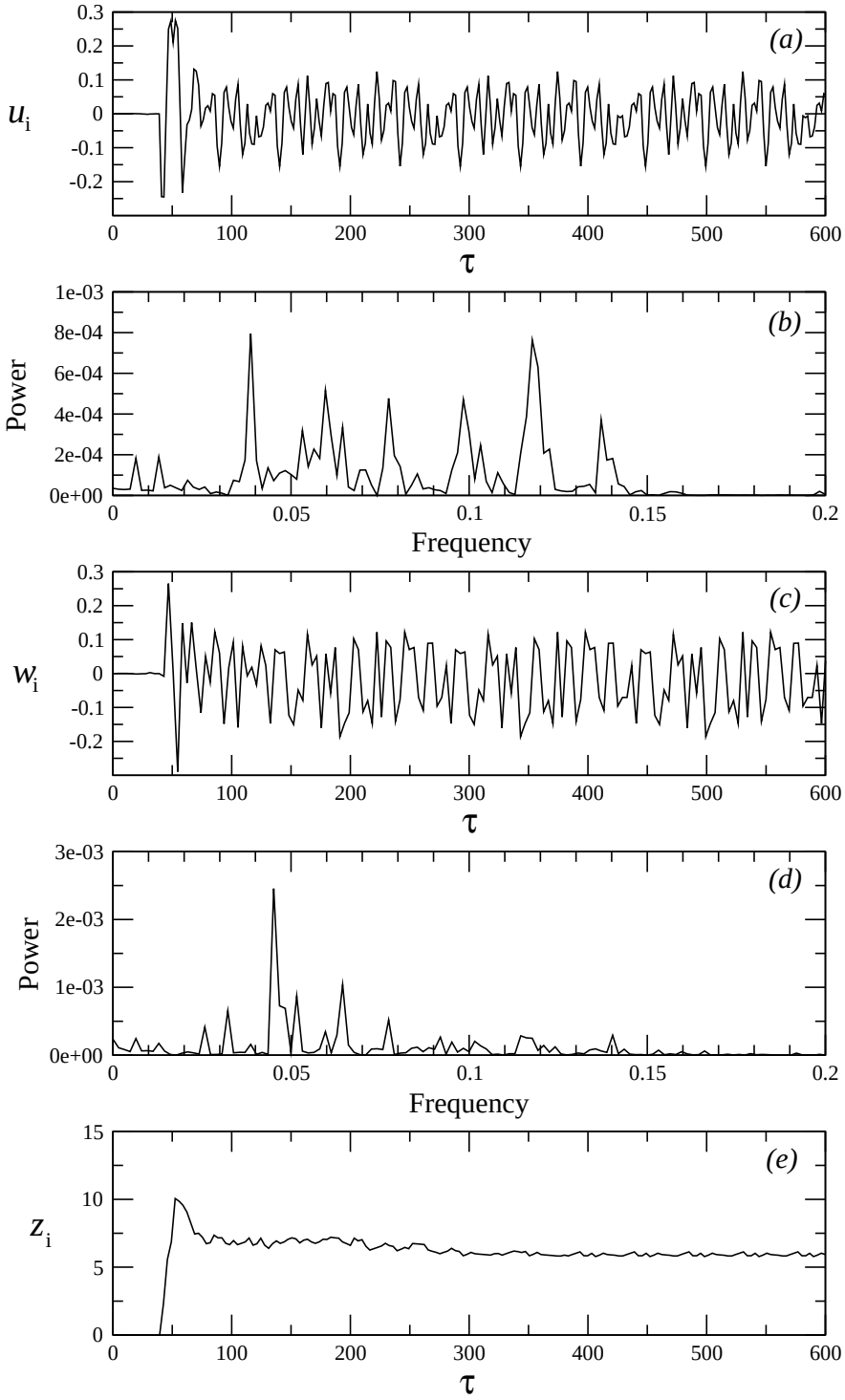

Figure 14: Time series of (a) u_i, (c) w_i, and (e) z_i of the twin round fountains at $Fr = 3$ and $Re = 400$ which demonstrate an unsteady strongly multi-modal interaction behavior, and the corresponding power spectra of u_i (b) and w_i (d), respectively.

3.2. Maximum fountain penetration heights and interaction thickness

The time series of the dimensionless maximum penetration heights of the twin transitional round fountains, *i.e.*, $z_{m,1}$ and $z_{m,2}$, and the dimensionless maximum thickness of the interaction region, z_i, on the plane passing through the two fountain sources are presented in Fig. 15 for the $Fr = 1$ fountains at $Re =$ 25, 50, 100, 200, 300 and 400, respectively, where $z_{m,1}$, $z_{m,2}$, and z_i are made dimensionless by X_0. It is seen from this figure that the time series of $z_{m,1}$ and $z_{m,2}$ for these $Fr = 1$ twin fountains are basically identical at each of the six Re values; all time series except that at $Re = 400$ demonstrate an oscillatory behavior at the initial stage of the development but attain steady states with constant values of $z_{m,1}$, $z_{m,2}$, and z_i after some periods of time; the time for these parameters to attain the steady state, τ_s, which is made dimensionless by (X_0/W_0), increases significantly with Re, from $\tau_s \approx 30$ at $Re = 25$ to $\tau_s \approx 270$ at $Re = 300$; however, the time series at $Re = 400$ does not attain a steady state as others do, remaining unsteady at full development; the magnitudes of $z_{m,1}$ and $z_{m,2}$, no matter at the initial development stage or at the steady state, increase with Re, which is in agreement with the results obtained by others as discussed in § 1; the magnitudes of z_i, no matter at the initial development stage or at the steady state (including quasi-steady state when $Re = 400$), also increase with Re, however, z_i is always smaller than $z_{m,1}$ and $z_{m,2}$ for each of the six Re cases.

A similar behavior is observed for higher Fr twin fountains. For example, Figures 16 and 17 present the time series of $z_{m,1}$, $z_{m,2}$, and z_i for the $Fr = 2$ twin fountains at $Re = 50$, 75, 100, 200, 300 and 400, and for $Fr = 5$ at $Re = 100$, 200, 300 and 400, respectively. It is clear that these two figures illustrate a similar behavior to that shown in Fig. 15. The only noticeable differences are that when Fr increases the bounding value of Re at which twin fountains can attain steady states, with constant $z_{m,1}$, $z_{m,2}$, and z_i after periods of initial development with oscillatory behavior, decreases from $Re = 300$ when $Fr = 1$ to $Re = 100$ when $Fr = 2$ and 5; the times to attain the steady states apparently increases with Fr, *e.g.*, at $Re = 100$, $\tau_s \approx 100$ for $Fr = 1$, $\tau_s \approx 150$ for $Fr = 2$, and $\tau_s \approx 200$ for $Fr = 5$; the magnitudes of $z_{m,1}$ and $z_{m,2}$ increase with Fr, which is also in

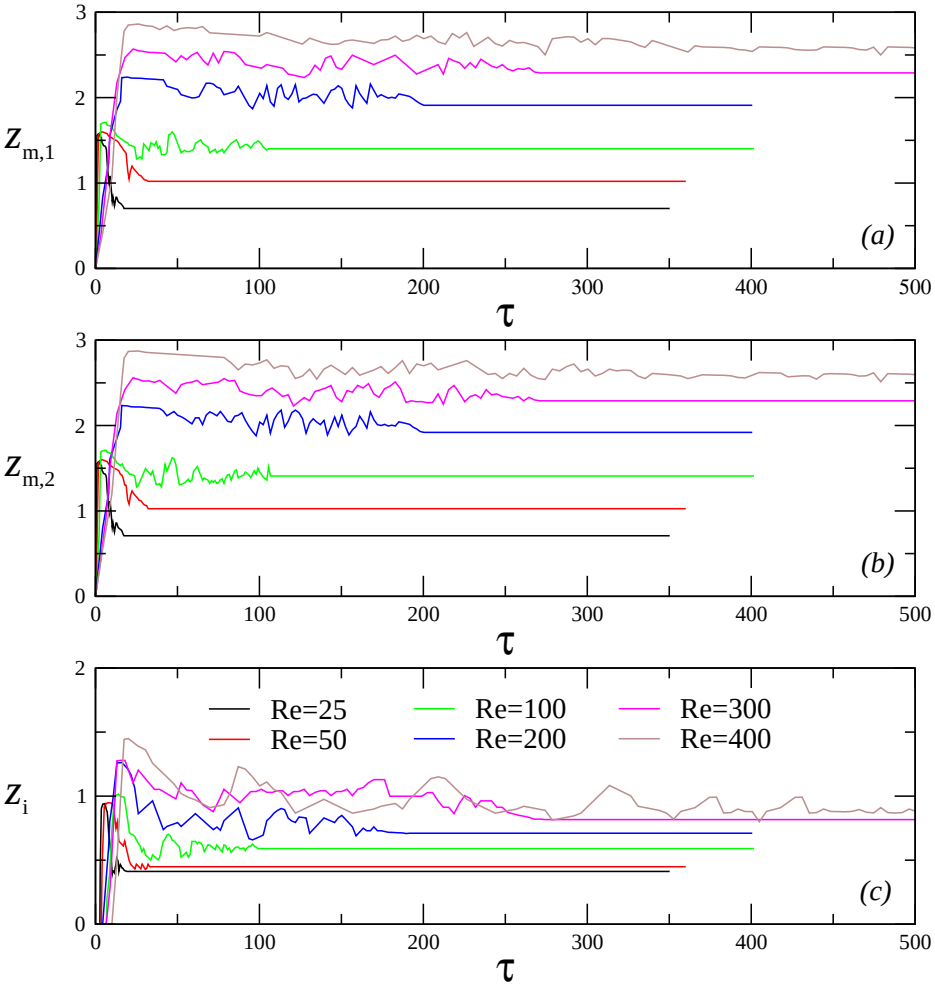

Figure 15: Time series of (a) $z_{m,1}$, (b) $z_{m,2}$, and (c) z_i of the $Fr = 1$ twin round fountains with Re in the range of 25 to 400.

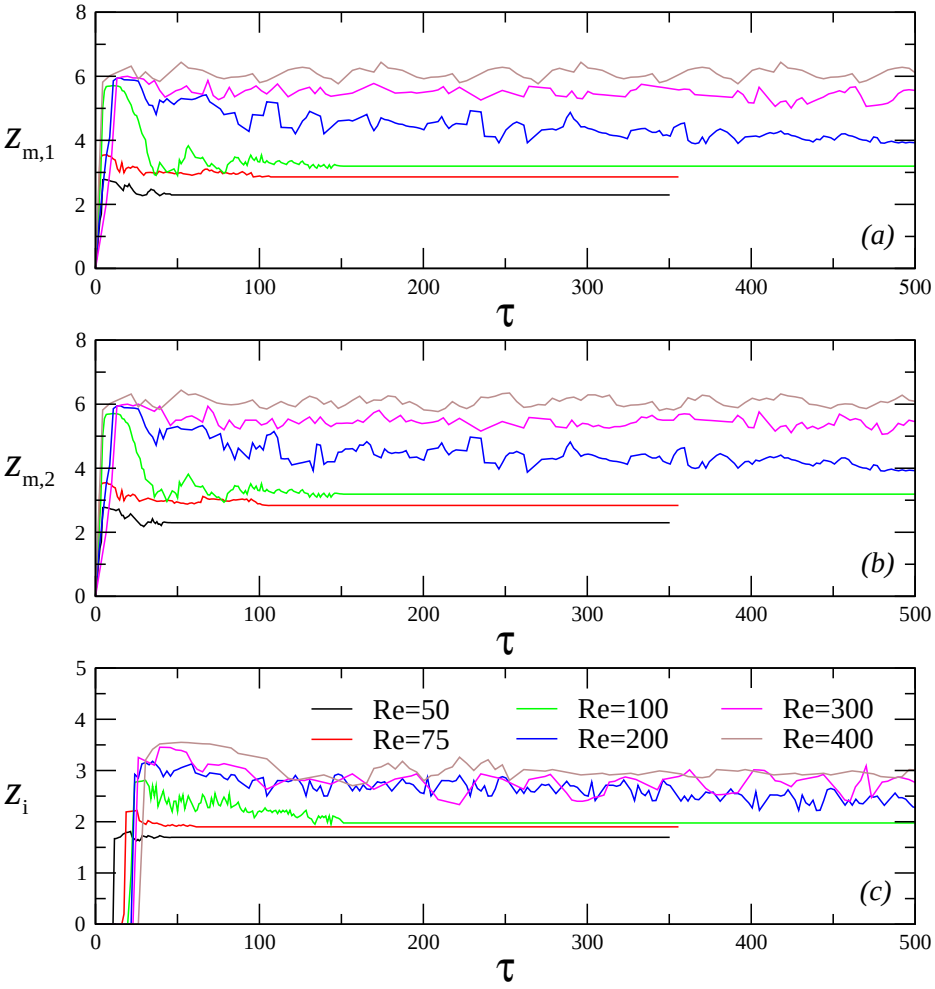

Figure 16: Time series of (a) $z_{m,1}$, (b) $z_{m,2}$, and (c) z_i of the $Fr = 2$ twin round fountains with Re in the range of 50 to 400.

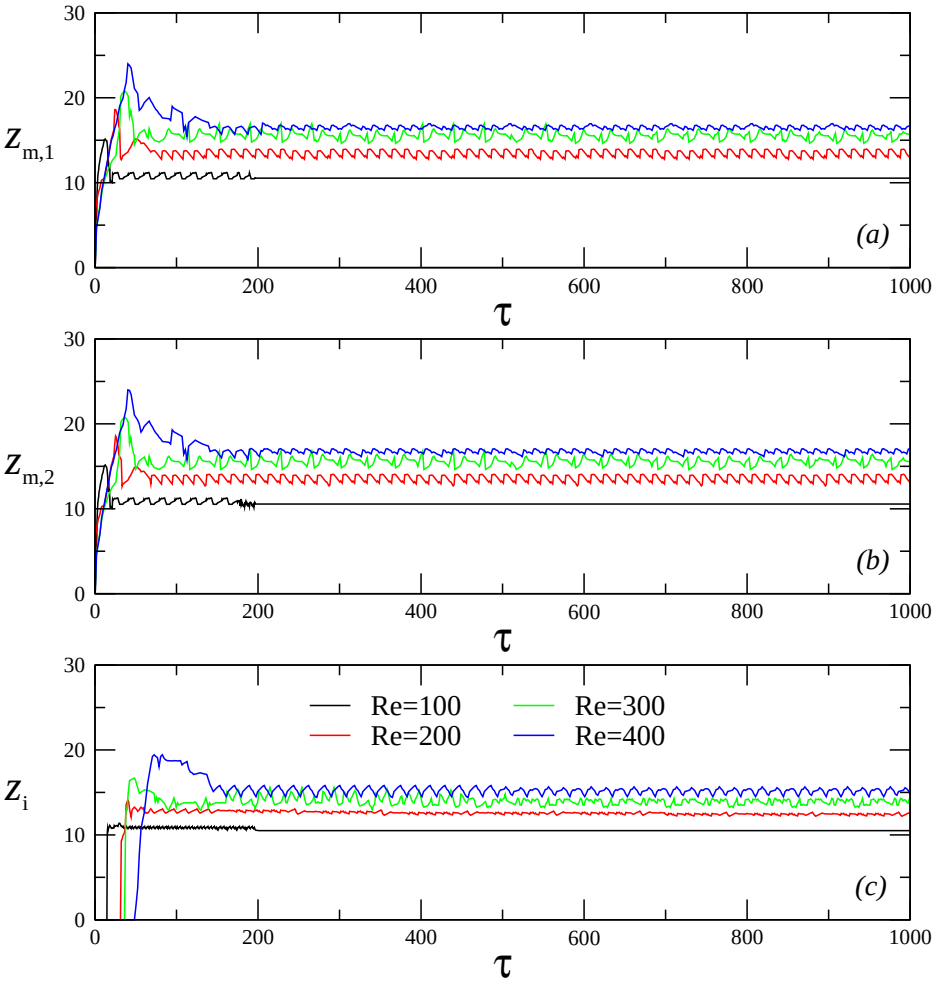

Figure 17: Time series of (a) $z_{m,1}$, (b) $z_{m,2}$, and (c) z_i of the $Fr = 5$ twin round fountains with Re in the range of 100 to 400.

agreement with the results obtained by others as discussed in § 1; and accordingly the magnitudes of z_i also increase with Fr.

As discussed in § 1, dimensional analysis can be used to develop a scaling relation between the maximum fountain penetration height of a single fountain and the relevant governing parameters, *i.e.*, Re, Fr, etc. A similar scaling relation between the maximum interaction thickness z_i of twin fountains at the steady state, or the time-averaged $\bar{z}_i$ for the unsteady at full development cases, of the interaction development and the relevant governing parameters of the flow can also be developed by a similar dimensional analysis.

It is apparent that the dimensional maximum interaction thickness Z_i at the steady state, or $\bar{Z}_i$, is dependent on the radius of the fountain sources, X_0, the fountain discharge velocity at the sources, W_0, the density of the fountain fluid at the sources, ρ_0, the kinematic viscosity of the fluid, ν, the reduced gravity between the fountains and the ambient fluid at source, $g^{'}$ ($g^{'} = g(\rho_0 - \rho_a)/\rho_0$, where ρ_a is the density of the ambient fluid), and the distance between the two fountain sources, D. A standard dimensional analysis using the Buckingham-Pi theorem leads to the following relation,

$$\bar{z}_i = \frac{\bar{Z}_i}{X_0} = f\left(Re, Fr, \frac{D}{X_0}\right). \tag{5}$$

In the case where a steady state interaction is attained, $\bar{z}_i$ is z_i at the steady state.

It is found that the experimental results of this study show that the maximum penetration height of each of the twin transitional round fountains considered here has similar scaling relations to those obtained by [8, 13, 18] for comparable Re and Fr. Hence only the results about the maximum interaction thickness of the twin transitional round fountains are presented here. Furthermore, due to the limitation of the experiment setup in which a fixed $D/X_0 = 10$ was used in all experiments, the effect of D/X_0 is not considered in this paper and hence only the dependence of $\overline{z}_i$ on Re and Fr is studied here.

Equation (5) can then be reduced to

$$\overline{z}_i = f(Re, Fr). \tag{6}$$

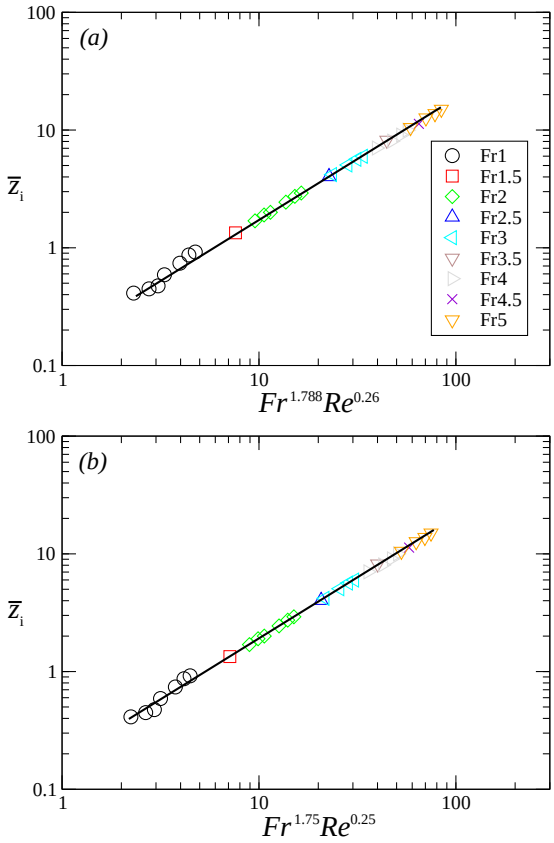

Figure 18: (a) $\bar{z}_i$ plotted against $Fr^{1.788}Re^{0.26}$ and (b) $\bar{z}_i$ plotted against $Fr^{1.75}Re^{0.25}$ for all twin round fountains considered. The straight line in (a) is the linear fit of the experimental data represented by $\bar{z}_i = 0.177Fr^{1.788}Re^{0.26}$ and the straight line in (b) is represented by $\bar{z}_i = 0.194Fr^{1.75}Re^{0.25}$, respectively.

The simplest way to determine the specific form of the scaling relation Eq. (6) for the interaction thickness of twin transitional round fountains studied here is to assume the following relation,

$$\overline{z}_i = aRe^b Fr^c, \tag{7}$$

where a, b and c are constants which were determined by a multiple linear regression technique applied to the experimental results. For the twin transitional round fountains studied in this study, the following specific scaling relation was obtained using the experimental results over the ranges of Re and Fr considered in this paper and at the fixed spacing of $D/X_0 = 10$,

$$\overline{z}_i = 0.177 Fr^{1.788} Re^{0.26}, \tag{8}$$

with a regression constant of 0.999, indicating this is an exceptionally good scaling relation, as clearly demonstrated in Fig. 18(a) where the experimentally obtained $\bar{z}_i$ is plotted against $Fr^{1.788}Re^{0.26}$.

It is interesting to note that the value of c obtained, *i.e.*, 0.26, is very close to 1/4, whereas the value of b obtained, *i.e.*, 1.788, is very close to 7/4. It is reasonable to speculate that in Eq. (7) b should be 7/4 and c should be 1/4 for the twin transitional round fountains at the ranges of Re and Fr studied in this study, as these values also produce an exceptionally good scaling relation between $\bar{z}_i$ and Re and Fr, which is given below, as shown in Fig. 18(b),

$$\overline{z}_i = 0.194 Fr^{7/4} Re^{1/4}, \tag{9}$$

with a regression constant of 0.997. In view of uncertainties associated with the measurement errors and the inevitable variations of fluid properties during the experiments, it is believed that Eqn. (9) is the more appropriate scaling relation to represent the dependence of $\bar{z}_i$ on Re and Fr over the parameter ranges considered in this paper. Nevertheless, it is apparent that further studies are necessary to find the underpinning physics to support this speculation.

4. Conclusions

Bobbing and flapping motions, which are the horizontal and vertical motions of the peak point of the interface between the interaction region and the ambient fluid on the vertical plane passing through the twin fountain sources, are found to be the dominant characteristics of the behavior of the interaction between twin transitional round fountains in a homogeneous fluid over the range of $25 \leq Re \leq 400$ and $1 \leq Fr \leq 5$ and at the fixed spacing of $D/X_0 = 10$, as demonstrated experimentally using a noninvasive PIV technique and flow visualization. Over the relatively narrow ranges of Re and Fr considered in this paper, the interaction behavior can be steady, unsteady and weakly multi-modal or unsteady and strongly multi-modal. In a steady case, the interaction exhibits the bobbing and flapping behavior only in the initial stage and attains a steady state in the later stage of the development in which these motions disappear and z_i becomes constant. In the unsteady regimes, the bobbing and flapping motions are present at all stages of the development of the interaction, which is then unsteady for all time. In the unsteady regimes, at full development, the horizontal and vertical velocities, and the interaction height, oscillate about an approximately constant, time averaged, value. The steady interaction behavior is observed for the cases with $Re \leq 100$ for all Fr values considered and for $Fr = 1$ with all Re values considered, except $Re = 400$. The unsteady weakly multi-modal interaction behavior is observed for $150 \leq Re \leq 300$ with $1.5 \leq Fr \leq 5$ and $Fr = 1$ with $Re = 400$, and the unsteady strongly multi-modal interaction behavior is found for $Re = 400$ with $1 < Fr \leq 5$.

A scaling relation between the maximum interaction thickness $\bar{z}_i$, for all regimes, and the governing parameters of the flow, *i.e.*, Re, Fr and D/X_0, was developed using a dimensional analysis. The specific scaling relation obtained using the experimental results of the current study found that $\bar{z}_i = 0.194 Fr^{7/4} Re^{1/4}$ for the twin transitional round fountains in a homogeneous ambient over the range of $25 \leq Re \leq 400$ and $1 \leq Fr \leq 5$, at the fixed spacing of $D/X_0 = 10$.

Acknowledgment

The authors would like to thank the anonymous reviewers for their constructive comments and suggestions. The financial support from the National Natural Science Foundation of China (51469035, 51266016), the Yunnan Natural Science Foundation (2011FA017), and the Australian Research Council (ARC) is gratefully acknowledged. H. M. also thanks James Cook University for the JCUPRS scholarship.

References

[1] B.R. Morton, Forced plumes, J. Fluid Mech. 5 (1959) 151–163.

[2] N. Srinarayana, S.W. Armfield, W. Lin, Impinging plane fountains in a homogeneous fluid, Int. J. Heat Mass Transfer 52 (2009) 2614–2623.

[3] N. Willianson, S.W. Armfield, W. Lin, Transition behavior of weak turbulent fountains, J. Fluid Mech. 655 (2010) 306–326.

[4] N. Srinarayana, N. Williamson, S.W. Armfield, W. Lin, Line fountain behavior at low-Reynolds number, Int. J. Heat Mass Transfer 53 (2010) 2065–2073.

[5] O.J. Myrtroeen, G.R. Hunt, Negatively buoyant projectiles – from weak fountains to heavy vortices, J. Fluid Mech. 657 (2010) 227–237.

[6] G. Carazzo, E. Kaminski, S. Tait, The rise and fall of turbulent fountains: a new model for improved quantitative predictions, J. Fluid Mech. 657 (2010) 265–284.

[7] N. Williamson, S. W. Armfield, W. Lin, Forced turbulent fountain flow behaviour, J. Fluid Mech. 671 (2011) 535–558.

[8] H.C. Burridge, G.R. Hunt, The rise heights of low- and high-Froude-number turbulent axisymmetric fountains, J. Fluid Mech. 691 (2012) 392–416.

[9] H.C. Burridge, G.R. Hunt, The rhythm of fountains: the lenghth and time scales of rise height fluctuations at low and high Froude number fountains, J. Fluid Mech. 728 (2013) 91–119.

[10] N. Srinarayana,S.W. Armfield, W. Lin, Behaviour of laminar plane fountains with a parabolic inlet velocity profile in a homogeneous fluid, Int. J. Thermal Sci. 67 (2013) 87–95.

[11] H.C. Burridge, G.R. Hunt, Scaling arguments for the fluxes in turbulent miscible fountains, J. Fluid Mech. 744 (2014) 273–285.

[12] B.R. Vinoth, P.K. Panigrahi, Characteristics of low Reynolds number non-Boussinesq fountains from non-circular sources, Phys. Fluids 26 (2014) 014106.

[13] N.B. Kaye, G.R. Hunt, Weak fountains, J. Fluid Mech. 558 (2006) 319–328.

[14] W. Lin, S. Armfield, Direct simulation of weak axisymmetric fountains in a homogeneous fluid, J. Fluid Mech. 403 (2000) 67–88.

[15] W. Lin, S. Armfield, Very weak fountains in a homogeneous fluid, Numer. Heat Transfer Part A: Appl. 38 (2000) 377–396.

[16] W. Lin, S. Armfield, The Reynolds and Prandtl number dependence of weak fountains, Comput. Mech. 31 (2003) 379–389.

[17] W. Lin, S.W. Armfield, Onset of entrainment in transitional round fountains, Int. J. Heat Mass Transfer 51 (2008) 5226–5237.

[18] N. Williamson, N. Srinarayana, S.W. Armfield, G.D. McBain, W. Lin, Low-reynolds-number fountain behaviour, J. Fluid Mech. 608 (2008) 297–318.

[19] H. Zhang, R.E. Baddour, Maximum penetration of vertical round dense jets at small and large Froude numbers, J. Hydraulic Eng. 124 (1998) 550–553.

[20] G. Abraham, Jets with negative buoyancy in homogeneous fluid, J. Hydraulic Research 5(4) (1967) 235–248.

[21] R.A. Seban, M.M. Behnia, K.E. Abreu, Temperatures in a heated air jet discharged downward, Int. J. Heat Mass Transfer 21 (1978) 1453–1458.

[22] L. Pantzlaff, R.M. Lueptow, Transient positively and negatively buoyant turbulent round jets, Exp. Fluids 27 (1999) 117–125.

[23] J.S. Turner, Jets and plumes with negative or reversing buoyancy, J. Fluid Mech. 26 (1966) 779–792.

[24] I.H. Campbell, J.S. Turner, Fountains in magma chambers, J. Petrology 30 (1989) 885–923.

[25] W.D. Baines, J.S. Turner, I.H. Campbell, Turbulent fountains in an open chamber, J. Fluid Mech. 212 (1990) 557–592.

[26] J.S. Turner, Bouyant plumes and thermals, Annu. Rev. Fluid Mech. 1 (1969) 29–44.

[27] E.J. List, Turbulent jets and plumes, Annu. Rev. Fluid Mech. 14 (1982) 189–212.

[28] L.J. Bloomfield, R.C. Kerr, Inclined turbulent fountains, J. Fluid Mech. 451 (2002) 283–294.

[29] G.R. Hunt, T. Van Den Bremer, Classical plume theory: 1937–2010 and beyond, IMA J. Applied Math. 76 (2011) 424–448.

[30] A. W. Woods, Turbulent plumes in nature, Annu. Rev. Fluid Mech. 42 (2010) 391–412.

[31] P.D. Friedman, J. Katz, Rise height for negatively buoyant fountains and depth of penetration for negatively buoyant jets impinging an interface, ASME J. Fluids Eng. 122 (2000) 779–782.

[32] P. Phillipe, C. Raufaste, P. Kurowski, P. Petitjeans, Penetration of a negatively buoyant jet in a miscible liquid, Phys. Fluids 17 (2005) 053601.

[33] L. Pera, B. Gebhart, Laminar plume interactions, J. Fluid Mech. 68 (1975) 259–271.

[34] B. Gebhart, H. Shaukatullah, L. Pera, The interaction of unequal laminar plane plumes, Int. J. Heat Mass Transfer 19 (1976) 7519–756.

[35] M. Brahimi, L. Dehmani, D.K. Son, Turbulent structure of the interacting flow of two thermal plumes, Int. J. Heat Mass Transfer 32 (1989) 1551–1559.

[36] C.Y. Ching, H.J.S. Fernando, L.A. Mofor, P.A. Davies, Interaction between multiple line plumes: a model study with applications to leads, J. Phys. Oceanogr. 26 (1996) 525–540.

[37] J.A. Davis, C.F. Lange, Simulations of three-dimensional buoyant laminar plumes in a Martian environment, Numer. Heat Transfer Part A: Appl. 62 (2012) 843–860.

[38] A.C.H. Lai, J.H.W. Lee, Dynamic interaction of multiple buoyant jets, J. Fluid Mech. 708 (2012) 539–575.

[39] W.D. Baines, J.S. Turner, Turbulent buoyant convection from a source in a confined region, J. Fluid Mech. 37 (1969) 51–80.

[40] A. Wagner, M. Klebe, C. Parker, Monitoring results of a naturally ventilated and passively cooled office building in Frankfurt, Germany, Int. J. Ventilation 6 (2007) 3–20.

[41] G.O. Hughes, R.W. Griffiths, Horizontal convection, Annu. Rev. Fluid Mech. 40 (2008) 185–208.

[42] P. Cooper, P.F. Linden, Natural ventilation of an enclosure containing two buoyancy sources, J. Fluid Mech. 311 (1996) 153–176.

[43] P.F. Linden, P. Cooper, Multiple sources of buoyancy in a naturally ventilated enclosure, J. Fluid Mech. 311 (1996) 177–192.

[44] N.B. Kaye, P.F. Linden, Coalescing axisymmetric turbulent plumes, J. Fluid Mech. 502 (2004) 41–63.

[45] N.B. Kaye, P.F. Linden, Colliding turbulent plumes, J. Fluid Mech. 550 (2006) 85–109.

[46] P.F. Linden, G.F. Lane-Serff, D.A. Smeed, Emptying filling boxes, the fluid mechanics of natural ventilation, J. Fluid Mech. 212 (1990) 309–315.

[47] A.B.D. Wong, R.W. Griffiths, Stratification and convection produced by multiple turbulent plumes, Dyn. Atmos. Oceans 30 (1999) 101–123.

[48] A.B. Shrinivas, G.R. Hunt, Transient ventilation dynamics induced by heat sources of unequal strength, J. Fluid Mech. 738 (2014) 34–64.

[49] H. Mahmud, W. Lin, W. Gao, S.W. Armfield, Y. He, Behavior of the interaction between twin transitional round fountains in a homogeneous fluid, Part 2: Numerical study, Int. J. Heat Mass Transfer (submitted, 2014).

[50] D. Cole, The splashing morphology of liquid-liquid impacts, PhD thesis, James Cook University, Townsville, Australia, 2007.